Journal of Electronics and Electrical Engineering
https://ojs.wiserpub.com/index.php/JEEE

UNIVERSAL WISER PUBLISHER

Research Article

Adaptive Neural Network-Based PID Controller Design for Velocity Control of an Internal Combustion Engine Using Back Propagation Technique

Quang Truc Dam

Capgemini Engineering, Research & Innovation Direction, 12 rue de la Verrerie, 92190 Meudon, France
E-mail: Quang-truc.dam@capgemini.com

Received: 27 August 2024; **Revised:** 8 November 2024; **Accepted:** 20 November 2024

Abstract: Precise velocity control in internal combustion engines (ICEs) is essential for optimizing performance, improving fuel efficiency, and minimizing emissions. However, the nonlinear dynamics and inherent uncertainties within ICE systems present substantial challenges for traditional control methods. In this paper, we propose an adaptive control strategy that integrates a Proportional-Integral-Derivative (PID) controller with Back Propagation Neural Networks (BPNNs) to effectively address these complexities. The proposed controller architecture consists of two key components: a BPNN to estimate modelling uncertainties, such as unknown friction and external disturbances affecting the ICE, and a primary PID controller responsible for velocity regulation. The BPNN functions as a dynamic estimator, continuously learning and adapting to changes in system dynamics, thereby enhancing the robustness and adaptability of the control system. By accurately capturing the nonlinearities and uncertainties inherent in ICEs, the BPNN contributes to improved control performance and system stability. To validate the effectiveness of the proposed approach, extensive numerical simulations are performed using MATLAB Simulink. These simulations encompass a range of operating conditions and scenarios to thoroughly evaluate the controller's performance. Additionally, the proposed method is compared to conventional PID control techniques found in the literature, with a focus on robustness, tracking accuracy, and disturbance rejection. The results indicate that the adaptive PID controller, incorporating BPNNs, outperforms traditional PID methods, delivering superior velocity regulation and disturbance rejection. Furthermore, the proposed approach demonstrates significant potential for real-world applications in ICE systems, providing enhanced control performance and efficiency. This study advances the field of control engineering by introducing an innovative adaptive control strategy tailored specifically for velocity control in internal combustion engines. Leveraging the capabilities of BPNNs to address uncertainties, this approach contributes to improved system performance and offers a promising direction for future advancements in engine control technologies.

Keywords: internal combustion engines (ICEs), proportional-integral-derivative (PID) controller, back propagation neural networks (BPNNs), adaptive control, Matlab-Simulink

1. Introduction

The internal combustion engine (ICE) has long been a cornerstone of modern engineering, playing a pivotal role in revolutionizing transportation and power generation since its development [1, 2, 3]. As a testament to human ingenuity, the

DOI: https://doi.org/10.37256/jeee.3220245581

ICE efficiently converts the chemical energy stored in fossil fuels into mechanical energy through controlled combustion within a confined space. Among the various types of internal combustion engines, the four-stroke ICE stands out as a key player in both automotive and industrial applications, renowned for its efficiency, reliability, and versatility.

The operation of four-stroke internal combustion engines is based on a systematic cycle consisting of intake, compression, power, and exhaust strokes, each carefully orchestrated to maximize energy extraction from the fuel while propelling machinery forward. This cyclic process not only ensures optimal power output but also reduces waste and minimizes environmental impact compared to alternative engine designs. The dominance of four-stroke engines in conventional and hybrid vehicles can be attributed to their superior energy efficiency when compared to two-stroke engines [1, 2, 3]. This efficiency advantage arises from the fact that a four-stroke engine generates power once every two revolutions, leading to lower fuel consumption compared to two-stroke engines, which complete a power stroke with every revolution. This fundamental difference in power generation has significant implications for fuel economy and emissions reduction.

In addition to better fuel efficiency, four-stroke engines offer the advantage of producing fewer emissions and delivering more consistent torque than their two-stroke counterparts. This performance benefit is due to the more complex design of four-stroke engines, which allows for optimized combustion processes and reduced energy losses. Spark ignition (SI) engines, a common type of four-stroke engine, primarily run on gasoline but can also utilize ethanol as an alternative fuel, demonstrating their energy versatility. The main components of SI engines, including the intake and exhaust manifolds, intake and exhaust valves, spark plug, piston, coolant, cylinder, crankcase, connecting rod, and crankshaft, all play critical roles in ensuring the engine's overall performance and efficiency.

Given the extensive deployment of internal combustion engines (ICEs) across a multitude of applications, the study of speed control for these engines has garnered considerable attention within the automation and control engineering communities. Speed control is a critical factor in enhancing the performance, efficiency, and reliability of ICEs, making the design of effective speed controllers a key area of research. Recent efforts have particularly focused on the implementation of Proportional-Integral-Derivative (PID) controllers that are specifically tailored to meet the unique demands of ICE systems [4, 5]. These controllers are known for their robustness and adaptability, providing a reliable solution for maintaining desired engine speeds across a wide range of operating conditions. By effectively managing speed variations, PID controllers contribute significantly to optimizing engine operation and improving fuel efficiency, which are essential for reducing emissions and extending engine life.

Beyond the use of PID controllers, a variety of advanced control techniques have been explored to further enhance the performance of ICEs. For instance, a sophisticated control system utilizing a linear quadratic regulator (LQR) approach has been developed for precise control of engine speed and torque. This method leverages first-order transfer functions with delay to manage the dynamic response of ICEs [6, 7, 8]. The LQR approach has been successfully implemented and validated across a broad spectrum of operating conditions, including both diesel and spark ignition engine dynamometer sets. This validation underscores the critical role that advanced control strategies play in ensuring smooth and efficient engine operation under varying load conditions, which is essential for both industrial applications and automotive engineering.

Moreover, the application of Model Predictive Control (MPC) has emerged as a highly promising direction for improving the accuracy and flexibility of ICE speed control systems [9, 10, 11, 12, 13]. MPC is particularly valued for its ability to predict future engine behaviour and adjust control inputs accordingly, making it highly effective in handling the complex and nonlinear dynamics of ICEs. Recent research has also introduced adaptive sliding mode controllers aimed at regulating the air-fuel ratio in ICEs [14], which is crucial for optimizing combustion efficiency and reducing emissions. Additionally, the integration of deep learning methodologies into MPC controller design [15] has demonstrated the potential of these innovative techniques to further optimize engine performance. By leveraging the predictive capabilities of MPC alongside the adaptive learning features of neural networks, these controllers can continuously improve their performance in real-time, leading to more efficient and reliable engine operation.

Furthermore, the exploration of Secure Deep Reinforcement Learning (SDRL) [16] represents a cutting-edge approach in the development of control strategies for ICEs. SDRL focuses on ensuring both optimal performance and operational safety, which are increasingly important as engines become more complex and integrated with other systems. This approach aims to create robust and reliable control strategies that can adapt to the evolving needs of modern ICEs, offering enhanced

performance while mitigating risks associated with operational uncertainties. Data-Driven Event-Triggered Adaptive Dynamic Programming Control is proposed in [17]

Collectively, these diverse approaches reflect the ongoing advancements in control engineering aimed at improving the efficiency, reliability, and environmental impact of internal combustion engines. By integrating traditional methods like PID and LQR with modern techniques such as MPC, deep learning, and reinforcement learning, researchers are pushing the boundaries of what is possible in ICE control, paving the way for more sophisticated and sustainable engine technologies in the future.

One of the primary challenges in controlling internal combustion engines lies in addressing uncertainties and unknown factors, in addition to the conventional control methods. An alternative approach to mitigate these issues involves utilizing observers to estimate the unmeasured signals and subsequently compensating for them within the controller. Similar methodologies have been explored in the literature, as seen in [18, 19, 20, 21, 22, 23]. This approach offers a robust solution to improve control performance by accounting for unknown dynamics, thus enhancing the system's reliability and stability under varying operational conditions.

Building on these advancements, this paper introduces a novel approach that harnesses the capabilities of back-propagation neural networks (BPNNs) to design an adaptive PID controller for speed control in internal combustion engines (ICEs). The framework of Backpropagation Neural Networks (BPNNs) utilized in this study adopts the structure of BPNNs introduced in [24, 25]. However, our approach introduces a state-of-the-art control design, facilitating adaptive gain tuning for the neural network as well as for the controller gains, details of which are elaborated in the control design section. By integrating the strengths of BPNNs with the proven effectiveness of PID control, this approach seeks to significantly improve the performance and adaptability of ICE speed control systems. The proposed method is intended to address the complexities and uncertainties inherent in ICE operation, offering a more robust and responsive control solution. Ultimately, this contribution is poised to advance the field of engine control technologies, driving the continued evolution and refinement of ICE management systems.

The structure of this paper is organized as follows: Section 2 introduces the dynamic model of an ICE and outlines the control problem associated with this system. Section 3 is dedicated to the primary contribution of the paper, which is the design of the proposed control strategy. In this section, we provide a detailed explanation of how the back-propagation neural network (BPNN) is utilized to develop the adaptive controller. Section 4 focuses on validating the efficiency of the proposed controller through simulation experiments on speed control for an ICE. To further demonstrate the effectiveness of our approach, we compare its performance with that of a conventional PID controller. The paper concludes with a discussion in Section 5 and final remarks in Section 6.

2. Dynamic model of an ICE

In this section, one shall introduce the dynamic model of an internal combustion engine (ICE) and briefly outline the primary control challenges associated with it. This overview sets the groundwork for developing effective control strategies aimed at improving engine efficiency and performance.

To facilitate a more streamlined and effective control design process, the dynamic model of an ICE is segmented into two primary sub-models. The first sub-model, known as combustion dynamics, encompasses a comprehensive set of equations that capture the entire sequence from air intake and fuel injection to the combustion phase. During combustion, the chemical energy in the fuel is converted into mechanical energy, generating torque that drives the crankshaft. This phase is crucial as it directly influences the engine's power output and efficiency. In [3, 18], the authors provide a thorough summary and detailed mathematical analysis of combustion dynamics in general.

The second sub-model, crankshaft dynamics, focuses on the mechanical behaviour of the crankshaft, which is driven by the torque generated during combustion. This sub-model provides insight into the rotational movement of the crankshaft, which is a direct reflection of the engine speed. The engine speed, therefore, is defined by the rotational velocity of the crankshaft and is a key parameter in assessing engine performance. By dividing the ICE dynamic model into these two sub-models, the control design process becomes more manageable, allowing for a targeted approach to optimizing each

component's performance and achieving more precise control over the engine's operation. This division not only aids in understanding the fundamental processes but also supports the development of more effective control strategies for enhancing engine efficiency and performance.

2.1 *Combustion dynamic model*

The combustion model starts by taking the air from the environment to send to the chamber, this controls the amount of air flowing into the engine in response to the driver's accelerator pedal action.

The mass flow rate ($\dot{m}_{air}$) is determined as following (1) [26]:

$$\dot{m}_{air} = \frac{A_{eff} P_{upstr}}{\sqrt{R T_{upstr}}} \Psi(P_{ratio}) \tag{1}$$

P_{ratio} is the ratio of the downstream pressure (P_{dowstr}) and upstream pressure (P_{upstr}) and is given in (2), R is the ideal gas constant, T_{upstr} is the upstream temperature:

$$P_{ratio} = \frac{P_{dowstr}}{P_{upstr}} \tag{2}$$

$\Psi(P_{ratio})$ is a function of P_{ratio} and calculated based on different flow conditions as given in the following:

$$\Psi(P_{ratio}) = \begin{cases} \sqrt{\gamma \left(\frac{2}{\gamma+1}\right)^{\frac{\gamma+1}{\gamma-1}}} & if: \ P_{ratio} < \left(\frac{2}{\gamma+1}\right)^{\frac{\gamma}{\gamma-1}} \\ \sqrt{\frac{2\gamma}{\gamma-1}\left(P_{ratio}{}^{\frac{2}{\gamma}} - P_{ratio}{}^{\frac{\gamma+1}{\gamma}}\right)} & if: \left(\frac{2}{\gamma+1}\right)^{\frac{\gamma}{\gamma-1}} < P_{ratio} < P_{\lim} \\ \frac{P_{ratio}-1}{P_{\lim}-1}\sqrt{\frac{2\gamma}{\gamma-1}\left(P_{\lim}{}^{\frac{2}{\gamma}} - P_{\lim}{}^{\frac{\gamma+1}{\gamma}}\right)} & if: P_{\lim} < P_{ratio} \end{cases} \tag{3}$$

$P_{\lim}$ is the limitation of pressure ratio, γ is the ratio of specific heats.

A_{eff} is the effect area, and calculated as following:

$$A_{eff} = \frac{\pi}{4} D_{thr}{}^2 C_{thr}(\theta_{thr}) \tag{4}$$

$$\theta_{thr} = \Theta_{ct_{thr}} \frac{90}{100} \tag{5}$$

θ_{thr} is the opening angle of the throttle vale (in degrees), $\Theta_{ct_{thr}}$ is the percentage of the throttle body that opens, D_{thr} is the diameter of the throttle at the opening, $C_{thr}(\theta_{thr})$ is the discharge coefficient.

To calculate fuel flow rate, one uses the fuel injector characteristics and the fuel injector pulse width. The fuel flow rate model is given as follows [3]:

$$\dot{m}_{fuel} = \frac{N S_{inj} P_{w_{inj}} N_{cyl}}{c_{ps} 1000 * 60} \tag{6}$$

where N is engine speed in rpm, S_{inj} is the Fuel injector slope, N_{cyl} is the number of engine cylinders, c_{ps} is the crankshaft revolutions per power stroke.

Let us now define the air-fuel ration (AFR) as following:

$$AFR = \frac{\dot{m}_{air}}{\dot{m}_{fuel}} \tag{7}$$

The air-fuel ratio represents the ratio between the intake air into the chamber and the fuel injected into the chamber, this value will determine the performance of combustion reaction in the chamber, for the different kind of fuels used for the ICE, there exists a ideal value of AFR, in which, since the AFR converge to this value, the fuel in the chamber will be burn 100%. Therefore, one of the objectives of controlling ICE is to control the AFR always remains in its ideal value.

In the SI engine the indicated torque means that the torque or power of the engine is evaluated in the scope of thermodynamics (pressure and volume of cylinder), not including any mechanical losses in the whole power development and transmission process conceptually illustrates pressure variation in a cylinder along with crankshaft rotation angle. This torque is calculated as follows [3]:

$$\tau_{indicated} = \frac{P_{indicated} * 60}{2\pi N} \tag{8}$$

where $P_{indicated}$ is the indicated power and can be calculated as:

$$P_{indicated} = \dot{m}_{fuel} * LHV \, \eta_{indicated} \tag{9}$$

$\eta_{indicated}$ is the charging efficiency indicated by the engine and is a function of engine speed and indicated torque as depicted in Figure 1, LHV is the fuel lower heating value.

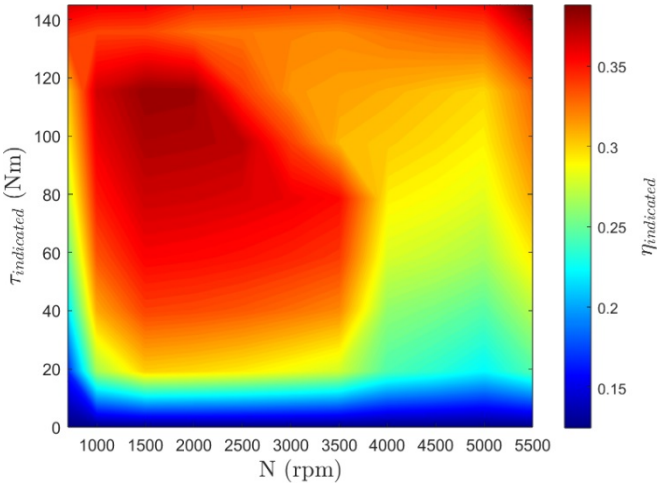

Figure 1. Indicated torque efficiency

2.2 *Crankshaft model*

The Crankshaft model demonstrates how the indicated torque generated by the combustion reaction inside the chamber acts on the crankshaft, which then cause the movement of crankshaft, hence generate the rotation movement of ICE. This relation is described as in the following equation:

$$\dot{\omega}(t) = -J^{-1}S(\omega)J\omega + J^{-1}\left(\tau_{control} + \tau_{uncertainties}\right) \tag{10}$$

where ω is the rotation rate of the ICE, J is the crankshaft's moment of initial, $\tau_{control}$ is the indicated torque, $\tau_{uncertainties}$ is the unknown factor such as friction, engine load. Because the crankshaft rotates in single axe, then we have $-J^{-1}S(\omega)J\omega = 0$, now set $\Gamma = J^{-1}\tau_{uncertainties}$, then we have the new dynamic equation of ICE is as:

$$\dot{\omega}(t) = J^{-1}\tau_{control} + \Gamma \tag{11}$$

Based on (6) and (8), (9) the (11) can be rewritten in a function of fuel flow rate as follows:

$$\dot{\omega}(t) = \frac{J^{-1}LHV\eta_{indicated}}{2\pi}\frac{S_{inj}N_{cyl}}{c_{ps}1000}P_{w_{inj}} + \Gamma \tag{12}$$

Hence, the objective of the control design in the following section is to regulate the fuel mass flow rate $\dot{m}_{fuel}$ by controlling $P_{w_{inj}}$ to ensure that the engine's rotational speed converges to its desired value, and to control the throttle valve opening angle to ensure complete combustion, maintaining 100% fuel burn efficiency after the combustion reaction. The method to determine the throttle valve opening angle will be detailed in the Appendix A.

3. Control design

The primary objective of this paper is to develop an adaptive controller for the system (12). To achieve this, the base controller will be designed using the Proportional-Integral-Derivative (PID) technique. Additionally, the unknown nonlinear external disturbances will be estimated using an adaptive neural network based on the back-propagation technique, as depicted in Figure 2. As previously discussed, the controller is structured into two primary components: speed control and air control. The air control component is designed to ensure complete combustion of the fuel, enhancing efficiency, and will be detailed in Appendix A. The core of the controller, however, lies in the speed control module, which is responsible for regulating fuel input to achieve the target trajectory. The subsequent sections will be dedicated to the development and formulation of this speed control module, outlining its design principles and operational mechanisms.

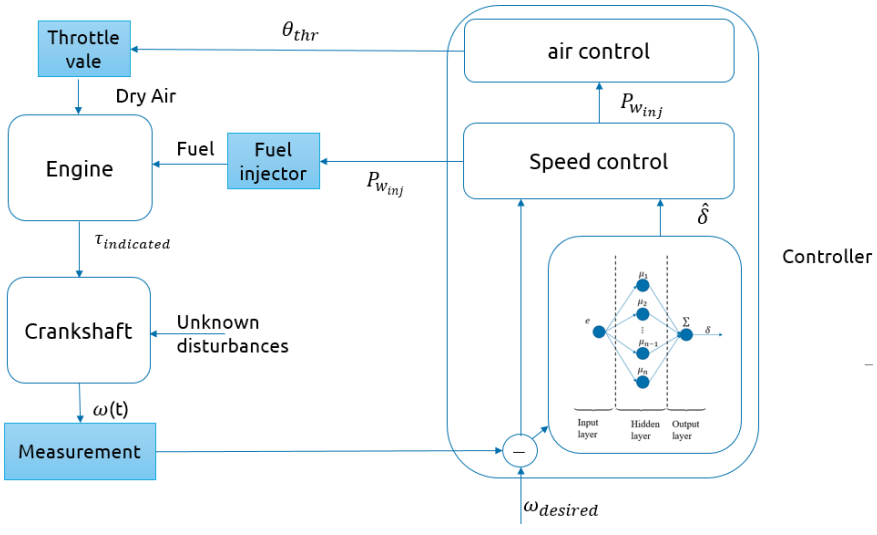

Figure 2. Control structure for controlling the ICE

Let us now reformulate the dynamic equation of Crankshaft from (12) as follows:

$$\dot{\omega}(t) = GP_{w_{inj}} + \Gamma \tag{13}$$

where $G = \frac{J^{-1} LHV \eta_{indicated}}{2\pi} \frac{S_{inj} N_{cyl}}{c_{ps} 1000} > 0$.

Now define the controller tracking error as following:

$$e = \omega_{desired} - \omega \tag{14}$$

From (13, 14) and set $U = P_{w_{inj}}$ one gets:

$$G^{-1}\dot{e} = -U - G^{-1}\Gamma + G^{-1}\dot{\omega}_{desired} \tag{15}$$

Let's define now $\delta = -G^{-1}\Gamma + G^{-1}\dot{\omega}_{desired}$ then (15) can be rewritten as follow:

$$G^{-1}\dot{e} = -U + \delta \tag{16}$$

Remark 1. *Given that the function δ is unknown, the control input U cannot be directly derived from Equation (16). To address this limitation, an artificial neural network utilizing the back-propagation (BPNN) technique will be employed to estimate the unknown function δ.*

3.1 *Neural network framework*

In this subsection, an artificial neural network using back-propagation technique will be exploited to estimate the unknown function δ as depicted in Figure 3. The neural network architecture consists of three primary layers: the input layer, followed by a hidden layer, and concluding with an output layer. The input layer serves as the entry point for data, where these data are received and passed on for processing, the data will be used in this study is the control error (e). The hidden layer, located between the input and output layers, performs the crucial task of transforming the input data by applying learned weights and activation functions. Finally, the output layer generates the final predictions based on the processed data from the hidden layer.

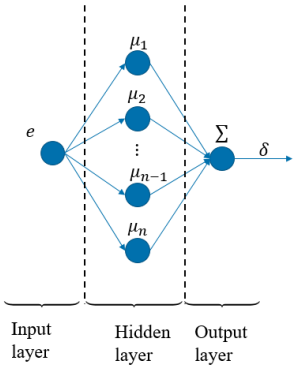

Figure 3. Neural network structure using in this paper

Indeed, as shown in many studies [24, 25], for ω restricted to a compact set and a neural network having a sufficiently number of hidden layers, δ can then be expressed as:

$$\delta = W\mu(\sigma e) + e_{NN} \tag{17}$$

where W is the ideal weigh matrix and e_{NN} is the approximation error, σ is the idea weight matrix of hidden layer, the hidden layer contains n node, the activation function of the hidden neurons and given as:

$$\mu_i(\sigma e) = \frac{2}{1 + exp(-2\sigma_i e)} - 1 \quad i = 1 \cdots n \tag{18}$$

$$\mu(\sigma e) = \begin{bmatrix} \mu_1(\sigma e) & \cdots & \mu_n(\sigma e) \end{bmatrix}^T \tag{19}$$

Note that from (18) one can obtain:

$$\|\mu_i(\sigma e)\| \leq 1 \tag{20}$$

Based on the neural network theory, since the number of nodes is chosen suitable, this approximation error will be bounded. However, the ideal weigh matric (W) is unknown, therefore, for calculating the estimation of δ one needs to estimate the value of W and σ, this estimation is given as $\widehat{W}$ and $\widehat{\sigma}$. Hence the estimation of δ is given as:

$$\widehat{\delta} = \widehat{W}\mu(\widehat{\sigma} e) \tag{21}$$

Based on this estimation, we propose the Robust controller using the Lyapunov theorem as follows:

$$U = K_1 e + K_2 \int e dt + K_3 sign(e) + \widehat{\delta} \tag{22}$$

To obtain the optimal estimation of δ, we must train the neural network together with the sliding mode controller while guaranteeing the convergence of $\widehat{W}$ and $\widehat{\sigma}$ to W and σ respectively. Therefore, in the following part, the details of designing $\widehat{W}$ and $\widehat{\sigma}$ will be given.

3.2 *Neural network design based on back-propagation technique*

In this section, a learning rule will be studied to train the defined network. Using the back-propagation technique, the basic update rules of weight matrices estimate can be given as follow:

$$\dot{\widehat{W}} = -\eta_w \frac{\partial S}{\partial \widehat{W}} - \rho_W \|e\| \widehat{W};\ \dot{\widehat{\sigma}} = -\rho_\sigma \|e\| \widehat{\sigma} \tag{23}$$

where $S = 0.5\, e^2$ is the objective cost function that should be minimized. η_w, ρ_W and ρ_σ are the training gains which will be design in next section.

Based on (23), the estimation of weight matrices can be deduced once the partial derivatives of cost function are solved.

By using the expression of the cost function and according to (21), we obtain:

$$\frac{\partial S}{\partial e} = e;\ \frac{\partial \widehat{\delta}}{\partial \widehat{W}} = \mu(\widehat{\sigma} e) \tag{24}$$

Based on (16), (21) and (22), one gets:

$$\frac{\partial G^{-1}\dot{e}}{\partial \widehat{\delta}} = -K_1 \frac{\partial e}{\partial \widehat{\delta}} - I \tag{25}$$

The Equation (25) presents a set of so-called back-propagation nonlinear dynamical systems, which will be solved to obtain the solutions of $\frac{\partial e}{\partial \widehat{\delta}}$. According to [4] and since the network converges relatively fast if the training gains are designed properly, then we can assume that the gradients have a static dynamic i.e., $\frac{\partial G^{-1}\dot{e}}{\partial \widehat{\delta}} = 0$. Hence, one gets:

$$\frac{\partial e}{\partial \widehat{\delta}} = \frac{-1}{K_1} \tag{26}$$

Now, let consider the decoupling of the partial derivatives $\frac{\partial S}{\partial \widehat{W}}$ as following:

$$\frac{\partial S}{\partial \widehat{W}} = \frac{\partial S}{\partial e} \times \frac{\partial e}{\partial \widehat{\delta}} \times \frac{\partial \widehat{\delta}}{\partial \widehat{W}} \tag{27}$$

Therefore, based on (24), (26) and (27), the rules of weight matrices (23) can be updated as:

$$\dot{\widehat{W}} = \frac{\eta_w}{K_1} e \mu^T (\widehat{\sigma} e) - \rho_W \|e\| \widehat{W};\ \dot{\widehat{\sigma}} = -\rho_\sigma \|e\| \widehat{\sigma} \tag{28}$$

The design of the control law (22) and the updating rules of the weight matrices (28) requires determining the controller gains K_1, K_2 and K_3 as well as the training parameters η_w, ρ_W and ρ_σ. In the next section, sufficient conditions involving the choice of these parameters to guaranty the stability of the overall control structure will be presented.

3.3 *Adaptive controller design*

The design of the control law (22) and the updating rules of the weight matrices (28) requires determining the controller gains K_1, K_2 and K_3 as well as the training parameters η_w, ρ_W and ρ_σ. In the next section, sufficient conditions involving the choice of these parameters to guaranty the stability of the overall control structure will be presented.

Before, stating our main results, we shall consider the following assumptions:

Assumption 1. *The disturbances δ is assumed to be unknown but bounded with known bounds i.e.,:*

$$\exists \varepsilon_\delta \in \mathbb{R}^+, \max_{t\geq 0} \|\delta\| \leq \varepsilon_\delta \tag{29}$$

Assumption 2 ([25])**.** *The ideal weight matrices W and σ are bounded i.e.,:*

$$\exists \varepsilon_W,\ \varepsilon_\sigma \in \mathbb{R}^+, \max_{t\geq 0} \|W\| \leq \varepsilon_W,\ \max_{t\geq 0} \|\sigma\| \leq \varepsilon_\sigma \tag{30}$$

Assumption 3 ([25])**.** *The ideal neural network estimation error e_{NN} is assumed small, unknown but bounded with known bounds:*

$$\exists \varepsilon_e \in \mathbb{R}^+, \max_{t\geq 0} \|e_{NN}\| \leq \varepsilon_e \tag{31}$$

Under the above assumptions, the next theorem will give sufficient conditions on the control gains K_1 and K_2 to ensure the stability of the ICE system (13) under the control law (22)

Theorem 1. *Consider the system (13) under the assumptions 1, 2, 3. If the controller (22) and the weight matrices gains η_w are chosen such that:*

$$K_1, K_2 > 0;\ \eta_w = K_1 \tag{32}$$

$$K_3 > max\left(\rho_W {\varepsilon_W}^2; \rho_\sigma {\varepsilon_\sigma}^2\right) + \varepsilon_e + 2\varepsilon_W \tag{33}$$

then, the stability of the closed-loop system will be globally ensured.

3.4 *Stability analyses*

Let define the estimation errors of weight matrices as $\widetilde{W} = W - \widehat{W},\ \widetilde{\sigma} = \sigma - \widehat{\sigma}$. Therefore, using the Equations (28), (32), the first derivative of these estimation errors w.r.t times can be expressed as:

$$\dot{\widetilde{W}} = -e\mu^T(\widehat{\sigma}e) + \rho_W \|e\| \left(W - \widetilde{W}\right);\ \dot{\widetilde{\sigma}} = \rho_\sigma \|e\| (\sigma - \widetilde{\sigma}) \tag{34}$$

Hence, from (17), (21) and (22), one can rewrite (16) as following:

$$G^{-1}\dot{e} = -K_1 e - K_2 \int e dt - K_3 sign(e) + \delta - \widehat{\delta} = -K_1 e - K_2 \int e dt - K_3 sign(e) + \widetilde{W}\mu(\widehat{\sigma}e) + \Delta \tag{35}$$

where $\Delta = e_{NN} + W(\mu(\sigma e) - \mu(\widehat{\sigma}e))$. From (20), (30) and (31) one can derive:

$$\|\Delta\| \leq \varepsilon_e + 2\varepsilon_W \tag{36}$$

Let consider now the following Lyapunov function:

$$V = \frac{1}{2}G^{-1}e^2 + \frac{1}{2}K_2\left(\int e dt\right)^2 + \frac{1}{2}tr\left(\widetilde{W}^T\widetilde{W}\right) + \frac{1}{2}tr\left(\widetilde{\sigma}^T\widetilde{\sigma}\right) \tag{37}$$

Based on (34), (35) one gets:

$$\begin{aligned} \dot{V} \quad &= e\left(-K_1 e - K_2 \textstyle\int e dt - K_3 sign(e) + \widetilde{W}\mu(\widehat{\sigma}e) + \Delta\right) + K_2 e \textstyle\int e dt \\ &- tr\left(\widetilde{W}^T e\mu^T(\widehat{\sigma}e) - \widetilde{W}^T\rho_W \|e\| \left(W - \widetilde{W}\right)\right) + tr\left(\widetilde{\sigma}^T\rho_\sigma \|e\| (\sigma - \widetilde{\sigma})\right) \end{aligned} \tag{38}$$

Using the fact that:

$$e\widetilde{W}\mu(\widehat{\sigma}e) - tr\left(\widetilde{W}^T e\mu^T(\widehat{\sigma}e)\right) = 0 \tag{39}$$

$$tr\left(\widetilde{W}^T\rho_W \|e\| \left(W - \widetilde{W}\right)\right) \leq -\rho_W \|e\| \left\|\widetilde{W}\right\|^2 + \rho_W \varepsilon_W \|e\| \left\|\widetilde{W}\right\| \tag{40}$$

$$tr\left(\widetilde{\sigma}^T\rho_\sigma \|e\| (\sigma - \widetilde{\sigma})\right) \leq -\rho_\sigma \|e\| \|\widetilde{\sigma}\|^2 + \rho_\sigma \varepsilon_\sigma \|e\| \|\widetilde{\sigma}\| \tag{41}$$

One gets the following:

$$\dot{V} \leq -K_1 e^2 - \|e\| \left(\rho_W \left\| \widetilde{W} \right\|^2 + \rho_\sigma \|\widetilde{\sigma}\|^2 \right) + \rho_W \varepsilon_W \|e\| \left\| \widetilde{W} \right\| + \rho_\sigma \varepsilon_\sigma \|e\| \|\widetilde{\sigma}\| - (K_3 - \Delta) \|e\| \tag{42}$$

From (33) and (36) one gets: $K_3 - \Delta > max\left(\rho_W {\varepsilon_W}^2; \rho_\sigma {\varepsilon_\sigma}^2\right)$. Hence one obtains

$$-\frac{1}{2} \|e\| \left(\rho_W \left\| \widetilde{W} \right\|^2 + \rho_\sigma \|\widetilde{\sigma}\|^2 \right) + \rho_W \varepsilon_W \|e\| \left\| \widetilde{W} \right\| + \rho_\sigma \varepsilon_\sigma \|e\| \|\widetilde{\sigma}\| - (K_3 - \Delta) \|e\| \leq 0 \tag{43}$$

Based on (43), we can derive the following Equation from (42)

$$\dot{V} \leq -K_1 e^2 - \frac{1}{2} \|e\| \left(\rho_W \left\| \widetilde{W} \right\|^2 + \rho_\sigma \|\widetilde{\sigma}\|^2 \right) \leq 0 \tag{44}$$

This ends the proof of Theorem 1

Remark 2. *As demonstrated in Equation (44), the stability of the proposed controller is ensured if the controller is designed according to Equations (32) and (33). However, it is important to note that the values of ρ_W and ρ_σ are not explicitly determined in the design process. These values directly influence the convergence speed, as indicated by the Lyapunov theorem and Equation (44). While higher values of ρ_W and ρ_σ can enhance convergence speed, they also tend to increase the chattering effect due to the use of the sign function. Therefore, the selection of ρ_W and ρ_σ should be tailored to the developer's requirements, balancing the need for fast convergence against the desire for smooth operation.*

Remark 3. *This approach is particularly advantageous as it effectively isolates all unidentified factors and model parameters from the control signal, allowing for the independent development of the controller. By decoupling these unknown elements from the control design process, we can focus on crafting a more precise and tailored control strategy without the direct influence of these uncertainties. It's worth noting that, in addition to employing Neural Networks (NN) to manage these unknown factors, there is another widely adopted method that involves the use of observers. Observers are specialized algorithms or systems designed to estimate unknown or unmeasured variables in dynamic systems. These observers, as detailed in [18, 19, 20, 21], provide an alternative or complementary approach to Neural Networks by offering real-time estimates of the unmeasured parameters, which can then be incorporated into the control strategy.*

Remark 4. *The controller proposed in this study, as demonstrated in Equation (22), operates independently of the specific model parameters. This characteristic makes the controller versatile, allowing it to be applied to a wide range of systems beyond just Internal Combustion Engine (ICE) systems. Its ability to function effectively without relying on predefined model parameters enhances its applicability across different types of dynamic systems, offering a robust solution for diverse control challenges.*

4. Simulation results

In this section, we will conduct a simulation validation of the proposed controller using MATLAB Simulink. The primary objective of these simulations is to showcase the controller's effectiveness in managing external unknown disturbances and parametric uncertainties that may influence the model. By simulating the system under various unknown disturbances, we aim to illustrate how well the proposed controller can maintain performance and stability despite these challenges. Additionally, we will compare the results with those obtained from a conventional PID controller. This comparison will highlight the advantages and improvements offered by our proposed approach, particularly in handling disturbances and uncertainties that are typically encountered in real-world applications. The parameter of ICE using in this simulation is given in Table 1.

Table 1. Parameter of ICE

Parameters	Values	Units
T_{upstr}	300	K
P_{upstr}	101,325	Pa
R	287	J/(kg·K)
γ	1.4	-
D_{thr}	50	mm
S_{inj}	6.4516	mg/ms
LHV	47,300,000	J/kg
N_{cyl}	4	-
c_{ps}	2	rev/stroke
J	0.6667	Kg·m^2

The simulation schema used for validating the proposed controller is illustrated in Figure 4 below, created within the MATLAB-Simulink platform. This model comprises several key components: ICE Model Block: This block simulates the dynamic behaviour of the internal combustion engine (ICE) based on the mathematical equations outlined in Section 2. It captures the engine's response to control inputs and external factors. ICE Controller Block: This block implements the controller designed in Section 3. It processes the input from the references block and adjusts the control signals to regulate the engine speed, compensating for disturbances and uncertainties. References Block: This block provides the desired reference values for the system, such as the target engine speed, which the controller aims to maintain. Environment Block: This block simulates external disturbances, friction, and environmental parameters such as temperature and pressure, which can impact the engine's performance. These factors are critical for testing the controller's ability to maintain stability and performance under varying conditions. This simulation setup provides a comprehensive platform to validate the proposed control strategy, ensuring that the controller can effectively manage the ICE's dynamic response under realistic operating conditions.

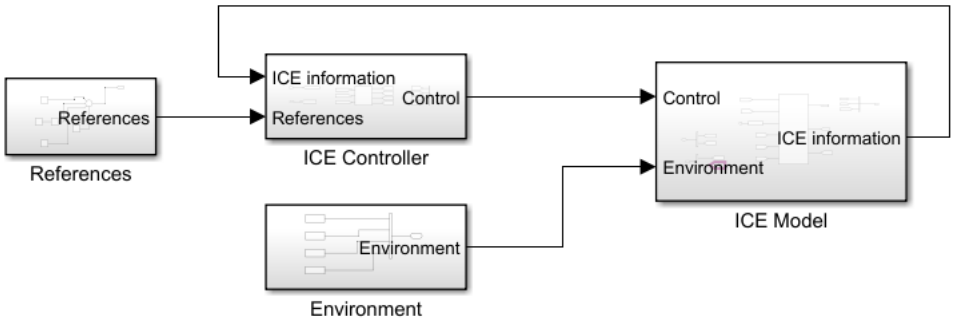

Figure 4. Simulation diagram in Matlab-Simulink

The objective of this study is to analyse the speed tracking performance of the proposed controller in comparison to a conventional PID controller, particularly under the influence of disturbances. To achieve this, the desired velocity tracking reference is illustrated in Figure 5. The engine's performance is evaluated under conditions of friction and external disturbances. Specifically, the friction effects impacting the engine are depicted in Figure 6A, while the external disturbances, including factors such as environmental variations and load changes, are shown in Figure 6B. These figures represent the challenges the controllers must overcome to maintain accurate speed tracking. The study aims to demonstrate the effectiveness of the proposed controller in managing these disturbances, ensuring superior speed tracking performance when compared to the traditional PID controller.

To ensure that the comparison remains fair, the controller in Equation (22) will be constructed with proportional-integral (PI) gains, denoted as K_1 and K_2, matching those used in the PI controller intended for the comparison. This alignment ensures consistency in the PI components across both controllers, facilitating a balanced evaluation of performance. The remaining components of the controller in Equation (22) will be configured according to the adaptive control law as outlined in Theorem 1. For comparison purposes, the controller used will be a PI controller, and its design parameters and specifications are detailed in the Appendix B. From this method we obtained $K_1 = K_P = 5.33$ and $K_2 = 1.267$.

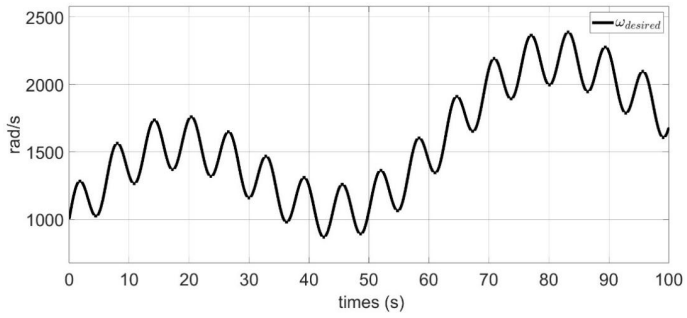

Figure 5. Desired value for conroller design

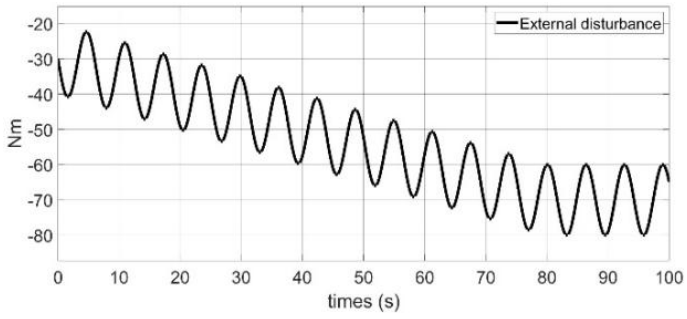

(A)

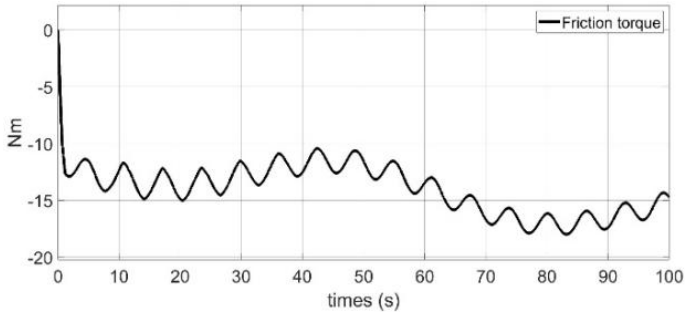

(B)

Figure 6. The friction torque (**A**) and external disturbance torque (**B**) affected to the system (10) during the simulation

The tracking control performances of both the PID controller and the BPNN-PID controller proposed in this study are illustrated in Figures 7 and 8. These figures demonstrate that all proposed controllers effectively accomplish the trajectory tracking task. However, a clear distinction emerges in the efficiency of the two approaches. The results from the PID controller reveal lower efficiency compared to the proposed BPNN-PID method. Notably, the controller introduced in this study maintains the internal combustion engine (ICE) at the desired speed with significantly reduced tracking error. This

finding highlights the superior performance of the proposed method in achieving precise speed control, emphasizing its potential to enhance operational stability and efficiency within the ICE system.

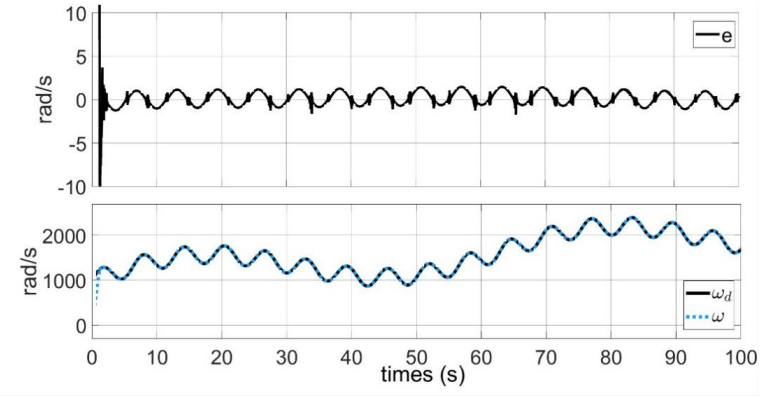

Figure 7. Simulation results for velocity tracking using BPNN PID controller

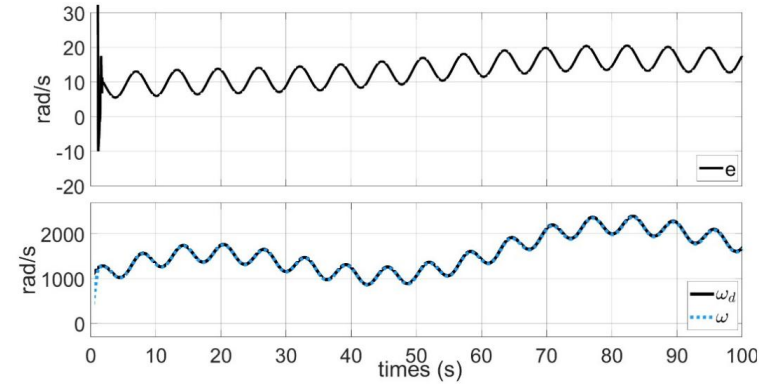

Figure 8. Simulation results for velocity tracking using PID controller

Figures 9 and 10 illustrate the output signals generated by the proposed controller and the traditional PID controller, respectively. In Figure 9, it is evident that the control signal produced by the proposed controller exhibits noticeable chattering effects. This chattering is a consequence of incorporating the sign function into the control strategy, as detailed in Remark 2. The use of the sign function, while beneficial for certain aspects of the control process, introduces rapid oscillations in the control signal, which manifest as chattering. These chattering effects are not only visible in the control signal but also have a direct impact on the tracking performance of the system. This is evident from the tracking error presented in Figure 7. The chattering in the control signal contributes to variations in the tracking error, highlighting a significant interplay between the control signal dynamics and the system's ability to follow the desired trajectory. The correlation between the chattering observed in the control signal and the tracking error underscores the broader implications of the sign function on the controller's performance.

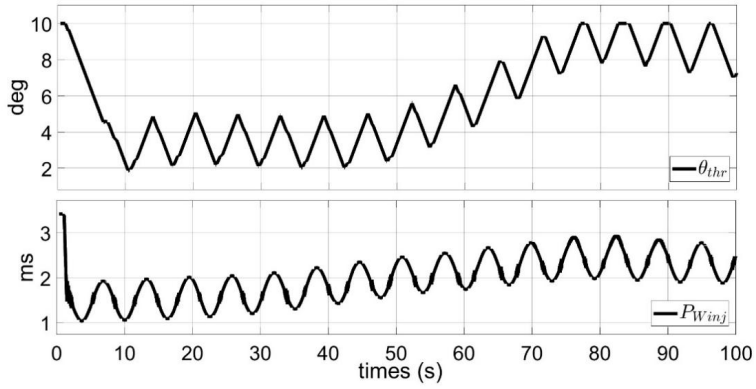

Figure 9. Control signal P_{w_inj} and throttle valve opening angle using BPNN PID

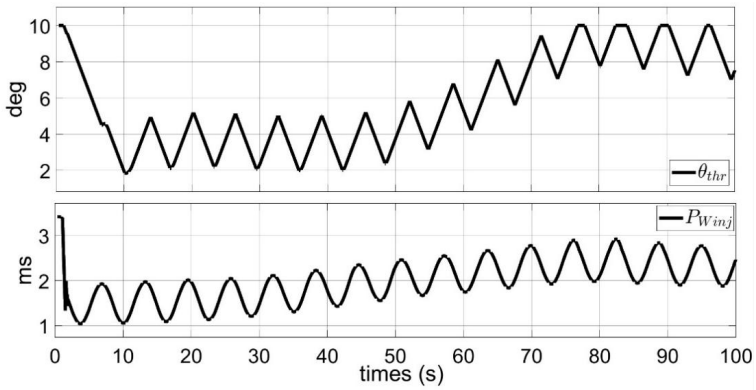

Figure 10. Control signal P_{w_inj} and throttle valve opening angle using PID

5. Discussion

The simulation results confirm the validity of the theoretical proposal presented in this work, demonstrating that the performance of the proposed controller surpasses that of the traditional PID controller. The data shows that the proposed controller effectively manages several aspects of the control process, delivering superior performance in comparison to the PID controller. However, a notable issue arises from the observed chattering effects in both the control signal and tracking performance. Specifically, the proposed controller exhibits significant chattering effects, which can adversely affect the smoothness of the control signal and, consequently, the precision of the tracking performance. These chattering effects are evident in the simulation results and suggest that while the proposed controller improves certain aspects of the control process, it introduces a trade-off in terms of signal smoothness and accuracy. These findings highlight the necessity for further investigation and refinement of the proposed control strategy to address and mitigate the chattering effects. Future research could focus on developing techniques to reduce or eliminate these oscillations, thereby enhancing the overall smoothness of the control signal and improving the tracking accuracy. By tackling these issues, the proposed controller could be optimized to deliver even better performance and stability, making it a more robust solution for speed control in internal combustion engines.

6. Conclusions

This paper introduces a novel adaptive controller designed to enhance speed control in ICE, effectively addressing the challenges posed by bounded disturbances, model uncertainties, and unknown parameters. The proposed controller, which integrates a traditional PID approach with an adaptive neural network employing back-propagation, demonstrates a significant advancement in control strategy by effectively estimating and compensating for unknown factors. The simulation results validate the efficacy of the proposed adaptive controller, revealing its superior performance in managing disturbances and uncertainties compared to a conventional PID controller. While the proposed controller shows notable improvements in handling complex dynamics and achieving desired speed control, the presence of chattering effects indicates areas for future refinement. These chattering effects, observed in both the control signal and tracking performance, highlight the need for further investigation to enhance the smoothness and precision of the control strategy. Overall, the proposed adaptive control method offers a robust and flexible solution for ICE speed control, demonstrating its potential to advance engine control technologies. Future work will focus on mitigating the chattering effects and further optimizing the controller to achieve even greater performance and stability. By addressing these challenges, the adaptive controller can be refined to provide more effective and reliable speed control in various practical applications, contributing to the continued evolution of engine management systems.

Conflict of interest

There is no conflict of interest for this study.

Appendix A

Based on the Equation (6) we can derive the desired fuel mass flow rate from the calculated control signal as follows:

$$\dot{m}_{fuel} = \frac{NS_{inj}UN_{cyl}}{c_{ps}1000 * 60} \tag{A1}$$

Based on (7), we can then determine the desired air mass flow rate as follows:

$$\dot{m}_{air} = \dot{m}_{fuel}AFR \tag{A2}$$

Then the desired effect area is determined based on (2) as follows:

$$A_{eff} = \frac{\dot{m}_{air}\sqrt{RT_{upstr}}}{P_{upstr}\Psi(P_{ratio})} \tag{A3}$$

Hence, based on (6), the desired open angle of throttle vale is given as:

$$\theta_{thr} = C_{thr}^{-1}\left(\frac{4A_{eff}}{\pi {D_{thr}}^2}\right) \tag{A4}$$

Appendix B

For controller design, let us recall the dynamic equation of the crankshaft as follows:

$$\dot{\omega}(t) = J^{-1}\tau_{control} + \Gamma \tag{A5}$$

The PI controller can be given as follows:

$$\tau_{control} = K_P e + K_I \int edt \tag{A6}$$

From (A5), (A6) we can determine the denominator of the transfer function of the close loop as follows:

$$D(s) = s^2 + J^{-1}K_P s + J^{-1}K_I \tag{A7}$$

Hence, we can determine $2\xi\omega_n = J^{-1}K_P$ and ${\omega_n}^2 = J^{-1}K_I$. Given the settling time T_s and the peak time T_p as follows:

$$T_s = \frac{4}{\xi\omega_n},\ T_p = \frac{\pi}{\omega_n\sqrt{|1-\xi^2|}} \tag{A8}$$

Now set the settling time $T_s = 1s$, and the peak time $T_p = 0.7s$, and consider the system is overdamped ($\xi > 1$) one gets: $K_P = 5.33,\ K_I = 1.267$

References

[1] M. Ehsani, Y. Gao, S. Longo, and K. Ebrahimi, *Modern Electric, Hybrid Electric, and Fuel Cell Vehicles*, 3rd ed. Boca Raton, FL, USA: CRC Press, Taylor & Francis Group, 2018.

[2] R. Stone, *Introduction to Internal Combustion Engines*, 2nd ed. Hampshire, UK: The Macmillan Press LTD, 1992.

[3] J. B. Heywood, *Internal Combustion Engine Fundamentals*, 2nd ed. New York, NY, USA: McGraw-Hill Education, 2018.

[4] N. S. Nise, *Control Systems Engineering*, 7th ed. Hoboken, NJ, USA: Wiley, 2015.

[5] D. Gao, Y. Lei, H. Zhu, and J. Ni, "Constant speed control of four-stroke micro internal combustion swing engine," *Chin. J. Mech. Eng.*, vol. 28, no. 5, pp. 971–982, 2015. https://doi.org/10.3901/CJME.2015.0512.070.

[6] R. Yang, X. Gong, Y. Hu, and H. Chen, "Motion control of free piston engine generator based on LQR," in *Proc. 34th Chin. Control Conf. (CCC)*, Hangzhou, China, Jul. 28–30, 2015, pp. 8091–8096. https://doi.org/10.1109/ChiCC.2015.7260927.

[7] M. Kang and T. Shen, "Experimental comparisons between LQR and MPC for spark-ignition engine control problem," in *Proc. 36th Chin. Control Conf. (CCC)*, Dalian, China, Jul. 26–28, 2017, pp. 2651–2656. https://doi.org/10.23919/ChiCC.2017.8027763.

[8] J. D. López, J. J. Espinosa, and J. R. Agudelo, "LQR control for speed and torque of internal combustion engines," *IFAC-PapersOnLine*, vol. 44, no. 1, pp. 2230–2235, 2011. https://doi.org/10.3182/20110828-6-IT-1002.02176.

[9] A. Norouzi, H. Heidarifar, M. Shahbakhti, C. R. Koch, and H. Borhan, "Model Predictive Control of Internal Combustion Engines: A Review and Future Directions," *Energies*, vol. 14, no. 19, p. 6251, 2021. https://doi.org/10.3390/en14196251.

[10] E. Shulga, P. Lanusse, T. B. Airimitoaie, S. Maurel, A. Trutet, "Model Predictive Control of engine intake manifold pressure with an uncertain model," *IFAC-PapersOnLine*, vol. 54, no. 6, pp. 335–340, 2021. https://doi.org/10.1016/j.ifacol.2021.08.566.

[11] D. Cairano, J. Doering, I. V. Kolmanovsky, and D. Hrovat, "Model Predictive Control of Engine Speed During Vehicle Deceleration," *IEEE Trans. Contr. Syst. Technol.*, vol. 22, no. 6, pp. 2205–2217, 2014. https://doi.org/10.1109/TCST.2014.2309671.

[12] G. Stewart and F. Borrelli, "A model predictive control framework for industrial turbodiesel engine control," in *Proc. 47th IEEE Conf. Decis. Control*, Cancun, Mexico, Dec. 9–11, 2008, pp. 5704–5711. https://doi.org/10.1109/CDC.2008.4739384.

[13] M. Keller, S. Geiger, M. Günther, S. Pischinger, D. Abell, and T. Albin, "Experimental Validation of Model Predictive Charging Pressure and EGR Rate Control for an SI Engine," in *Proc. IEEE Conf. Control Technol. Appl. (CCTA)*, Montreal, QC, Canada, Aug. 24–26, 2020, pp. 415–422. https://doi.org/10.1109/CCTA41146.2020.9206287.

[14] J. S. Souder and J. K. Hedrick, "Adaptive sliding mode control of air—fuel ratio in internal combustion engines," *Intl. J. Robust Nonlinear*, vol. 14, no. 6, pp. 525–541, 2004. https://doi.org/10.1002/rnc.901.

[15] A. Norouzi, S. Shahpouri, D. Gordon, A. Winkler, E. Nuss, D. Abel, et al. "Deep Learning based Model Predictive Control for Compression Ignition Engines," *Control Eng. Pract.*, vol. 127, p. 105299, 2022. https://doi.org/10.48550/ARXIV.2204.00139.

[16] A. Norouzi, S. Shahpouri, D. Gordon, M. Shahbakhti, and C. R. Koch, "Safe deep reinforcement learning in diesel engine emission control," *J. Syst. Control Eng.*, vol. 237, no. 8, pp. 1440–1453, 2023. https://doi.org/10.1177/09596518231153445.

[17] M. Shen, X. Wang, S. Zhu, Z. Wu, and T. Huang, "Data-Driven Event-Triggered Adaptive Dynamic Programming Control for Nonlinear Systems with Input Saturation," *IEEE Trans. Cybernet.*, vol. 54, no. 2, pp. 1178–1188, Feb. 2024. https://doi.org/10.1109/TCYB.2023.3337779.

[18] Q. T. Dam, R. E. H. Thabet, S. A. Ali, F. Guérin, and H. A. Ghani, "A High-Gain Observer Design for Nonlinear System with Delayed Measurements: Application to a Quadrotor UAV," *IFAC-PapersOnLine*, vol. 56, no. 2, pp. 6739–6744, 2023. https://doi.org/10.1016/j.ifacol.2023.10.379.

[19] Q. T. Dam, R. E. H. Thabet, S. A. Ali, and F. Gueri, "Observer Design for a Class of Uncertain Nonlinear Systems With Sampled-Delayed Output Using High-Gain Observer and Low-Pass Filter: Application for a Quadrotor UAV," *IEEE Trans. Ind. Electron.*, vol. 71, no. 1, pp. 933–942, 2024. https://doi.org/10.1109/TIE.2023.3247786.

[20] Q. T. Dam, R. El Houda Thabet, S. A. Ali, F. Guerin, and A. Hugo, "Filtered High-Gain Observer Design For a Class of Nonlinear Systems subject to Delayed Measurements: Application to a Quadrotor UAV," in *Proc. 2022 Amer. Control Conf. (ACC)*, Atlanta, GA, USA, Jun. 8–10, 2022, pp. 4050–4055. https://doi.org/10.23919/ACC53348.2022.9867537.

[21] Q. T. Dam, R. El Houda Thabet, S. A. Ali, F. Guerin, and A. Hugo, "Continuous—Discrete Time High Gain Observer Design for State and Unknown Inputs Estimations of Quadrotor UAV," in *Proc. Eur. Control Conf. (ECC)*, Delft, The Netherlands, Jun. 29–Jul. 2, 2021, pp. 1181–1186. https://doi.org/10.23919/ECC54610.2021.9655232.

[22] M. Shen, Y. Ma, J. H. Park, and Q. -G. Wang, "Fuzzy Tracking Control for Markov Jump Systems With Mismatched Faults by Iterative Proportional—Integral Observers," *IEEE Trans. Fuzzy Syst.*, vol. 30, no. 2, pp. 542–554, Feb. 2022. https://doi.org/10.1109/TFUZZ.2020.3041589.

[23] M. Shen, T. Zhang, J. H. Park, Q.-G. Wang, and L.-W. Li, "Iterative Proportional-Integral Interval Estimation of Linear Discrete-Time Systems," *IEEE Trans. Autom. Control.*, vol. 68, no. 7, pp. 4249–4256, July 2023. https://doi.org/10.1109/TAC.2022.3203226.

[24] Q. T. Dam, R. E. H. Thabet, S. A. Ali, F. Guerin, and Y. Tang, "Adaptive Neural Network-Based Sliding Mode Controller for Trajectory Tracking of A Quadrotor UAV," *Authorea Preprints*, 2023. https://doi.org/10.36227/techrxiv.24174771.v1.

[25] F. Abdollahi, H. Talebi, and R. Patel, "A stable neural network-based observer with application to flexible-joint manipulators," *IEEE Trans. Neural Netw.*, vol. 17, no. 1, pp. 118–129, 2006.

[26] J. B. Heywood, *Internal Combustion Engine Fundamentals*. New York, NY, USA: McGraw-Hill, 1998.